

Orbital perturbation coupling of primary oblateness and solar radiation pressure

Martin Lara · Elena Fantino · Roberto Flores

the date of receipt and acceptance should be inserted later

Abstract Solar radiation pressure can have a substantial long-term effect on the orbits of high area-to-mass ratio spacecraft, such as solar sails. We present a study of the coupling between radiation pressure and the gravitational perturbation due to polar flattening. Removing the short-period terms via perturbation theory yields a time-dependent two-degree-of-freedom Hamiltonian, depending on one physical and one dynamical parameter. While the reduced model is non-integrable in general, assuming coplanar orbits (i.e., both Spacecraft and Sun on the equator) results in an integrable invariant manifold. We discuss the qualitative features of the coplanar dynamics, and find three regions of the parameters space characterized by different regimes of the reduced flow. For each regime, we identify the fixed points and their character. The fixed points represent frozen orbits, configurations for which the long-term perturbations cancel out to the order of the theory. They are advantageous from the point of view of station keeping,

allowing the orbit to be maintained with minimal propellant consumption. We complement existing studies of the coplanar dynamics with a more rigorous treatment, deriving the generating function of the canonical transformation that underpins the use of averaged equations. Furthermore, we obtain an analytical expression for the bifurcation lines that separate the regions with different qualitative flow.

Keywords Hamiltonian dynamics, perturbation theory, Lie transforms, bifurcation theory, solar radiation pressure, oblateness perturbation

1 Introduction

The dynamics of natural and artificial bodies in the solar system is dominated by the Keplerian attraction of either the Sun or a different natural massive body. However, perturbations such as the non-sphericity of the primary body, tidal effects, or solar radiation pressure, may accumulate with time yielding notable changes with respect to Keplerian dynamics. For objects with high area-to-mass ratio, radiation pressure is an important effect [72, 75, 71, 8]. An example is the dust dynamics in planetary rings [56, 74]. Of special relevance for space technology are solar sails, a potential means of efficient spacecraft propulsion [60, 32].

The impact of radiation pressure has been acknowledged since the beginning of the space era. In particular, it was identified as the cause of disagreement between the predicted trajectory and the observed behavior of Vanguard I¹ [67] and, most notably, the Echo satellites²

A preliminary version of this research was presented at the Third International Nonlinear Dynamics Conference—NODYCON 2023 held in Rome, Italy, 18–22 June 2023 [52].

M. Lara
Scientific Computation and Technical Innovation Center, University of La Rioja, 26006 Logroño, Spain
Tel.: +34-941-299440
Fax: +34-941-299460
E-mail: mlara0@gmail.com

E. Fantino
Aerospace Engineering Department, and Space Technology and Innovation Center, Khalifa University of Science and Technology, P.O. Box 127788 Abu Dhabi, United Arab Emirates
E-mail: elena.fantino@ku.ac.ae (corresponding author)

R. Flores
Aerospace Engineering Department, Khalifa University of Science and Technology, P.O. Box 127788 Abu Dhabi, United Arab Emirates

¹ nssdc.gsfc.nasa.gov/nmc/spacecraft/1958-002B; last accessed December 25, 2023

² <https://space.jpl.nasa.gov/msl/QuickLooks/echoQL>; last accessed December 25, 2023

[70, 77, 36, 79]. This motivated theoretical research on its effects over the long-term motion of spacecraft [66, 42, 14, 1]. In spite of the non-conservative character of radiation pressure, it can be approximated with a disturbing potential. Under this simplification, the problem may be approached with Hamiltonian dynamics, which is particularly useful in the context of resonant motion [66, 39, 7, 24, 35].

The long-term effects of radiation pressure in high area-to-mass objects have been described analytically with a surrogate integrable dynamics [62, 63, 20, 61, 10]. The coupling with oblateness alters significantly the long-term dynamics [66, 7, 30, 31, 45, 23]. This opens opportunities for the design of novel mission orbits [13], including deorbiting strategies [29, 59].

The characterization of the coupled effect of the central-body oblateness and radiation pressure perturbations is, to our knowledge, still incomplete. Even in the simplest approach of the cannonball model [46] with constant solar flux and negligible solar parallax [42], which results in constant acceleration, the long-term behavior is governed by a time-dependent, two-degree-of-freedom system whose closed-form solution is not known. Notwithstanding the lack of a general solution, the dynamics of specific resonances have been discussed in detail [2, 29]. For the special case when the Sun lies on the equatorial plane, the coplanar orbits become an invariant manifold of the averaged problem. After truncation of higher-order effects, the reduced Hamiltonian depends on one physical and one dynamical parameter. Then, the general characteristics of the reduced flow can be studied in the plane of these parameters.

The standard analysis in literature starts directly from the averaged equations of orbital evolution. Then, the types of motion arising from different relative strengths of the governing parameters are studied. We establish a more formal framework for the problem with a complete canonical perturbation approach. We build the generating function of the infinitesimal contact transformation that removes the short-period terms from the original Hamiltonian [73, 25]. It provides the necessary theoretical foundation for the averaging assumptions [3], and enables the computation of higher-order solutions [6, 44, 21, 11, 26, 54, 49]. Beyond the qualitative description of the dynamics, the transformation between initial conditions and corresponding averaged variables is needed to initialize the constants of the perturbation theory. Their accurate computation is critical for the correct propagation of the long-term dynamics [9, 57, 78, 5, 50].

In the same spirit, seeking rigorous description of the typologies of motion, we derive analytical expressions for the fundamental lines of the parameters plane that separate regions with different types of flow. This

gives a formal underpinning to the mechanisms controlling changes in the flow, both local—bifurcations of relative equilibria—and global—related to the evolution of orbits that eventually become circular—. We demonstrate a complete description of the reduced phase space in terms of arithmetic operations only: the fundamental lines are determined computing discriminants of polynomial equations and applying Descartes’ rule of signs. For each regime, we identify the fixed points and their character. These points represent frozen orbits, configurations where the long-term effects of radiation pressure and oblateness cancel out to the order of the theory. Therefore, while short-term perturbations (i.e., with a periodicity of one orbit) persist, the secular drift of the orbital elements vanishes. This has the potential to extend spacecraft operational life, allowing for long-term station keeping with minimal propellant consumption.

Another original contribution is the derivation of the averaged equations in vectorial form. It is free from singularities and enhances the stability of numerical integration [55, 76]. Even though it introduces redundancy in the averaged differential system, computational cost does not increase because the symmetry of the equations allows for an efficient implementation.

The paper is organized as follows. After justifying the simplifications that yield the approximate Hamiltonian in §2, the perturbation solution is approached in §3, where the elimination of short-period terms provides a compact set of variation equations in vectorial form that can be efficiently integrated semi-analytically. Finally, the dynamics of the coplanar manifold are discussed in detail in §4. The Wolfram Mathematica software provided assistance with mathematical manipulations and plotting of results.

2 Perturbation model

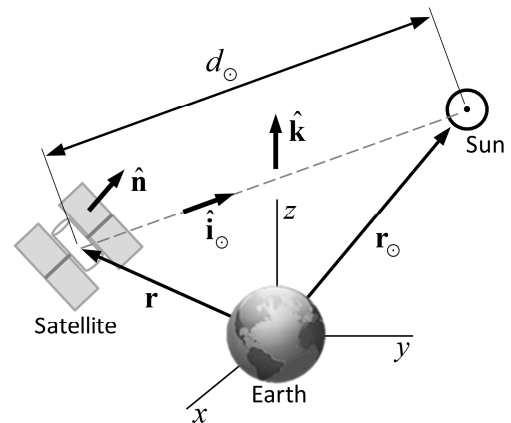


Fig. 1 Vectors and distances used in the perturbation model.

We focus on the case of a negligible mass object, the “orbiter”, moving around an oblate central body, the “planet”, at a distance where the tidal forces of the Sun, which we assume to revolve with Keplerian motion in its apparent orbit about the planet, are small compared to both radiation pressure and the effect of planetary oblateness. That is, $r/d_\odot \ll 1$, where

$$r = \sqrt{\mathbf{r} \cdot \mathbf{r}}, \quad (1)$$

$$d_\odot = \sqrt{(\mathbf{r}_\odot - \mathbf{r}) \cdot (\mathbf{r}_\odot - \mathbf{r})}, \quad (2)$$

and \mathbf{r} and \mathbf{r}_\odot denote the position vectors of the orbiter and the Sun, respectively, measured from the center of mass of the planet (see Fig. 1). In what follows, hats over vectors will denote directions. In particular,

$$\hat{\mathbf{r}} = \frac{\mathbf{r}}{r}, \quad \hat{\mathbf{r}}_\odot = \frac{\mathbf{r}_\odot}{r_\odot}, \quad (3)$$

with $r_\odot = \sqrt{\mathbf{r}_\odot \cdot \mathbf{r}_\odot}$.

Note that, due to the assumption of Keplerian motion, the planet-Sun distance is given by the polar equation

$$r_\odot = \frac{a_\odot(1 - e_\odot^2)}{1 + e_\odot \cos f_\odot}, \quad (4)$$

where the semimajor axis a_\odot and the eccentricity e_\odot of the solar orbit are constant. The computation of the true anomaly $f_\odot = f_\odot(t; a_\odot, e_\odot)$ requires the solution of Kepler’s equation [16].

The contribution of the planet oblateness to the potential is given by the second-degree zonal harmonic, whose dimensionless coefficient is denoted J_2 :

$$\mathcal{V}_{J_2} = \frac{\mu}{r} J_2 \frac{\alpha^2}{r^2} P_2(\hat{\mathbf{r}} \cdot \hat{\mathbf{k}}), \quad (5)$$

where μ is the gravitational parameter of the planet, α its equatorial radius and $\hat{\mathbf{k}}$ is a unit vector in the direction of the polar axis of the primary. Hereafter, we represent a Legendre polynomial of degree i as P_i . In particular,

$$P_2 = -\frac{1}{2} + \frac{3}{2}(\hat{\mathbf{r}} \cdot \hat{\mathbf{k}})^2. \quad (6)$$

For a flat plate, the acceleration due to radiation pressure is given by [64, 65]

$$\begin{aligned} \mathbf{a}_{\text{srp}} = & -\mathcal{P}_{\text{au}} \frac{\text{au}^2}{d_\odot^2} \frac{A}{m} (\hat{\mathbf{l}}_\odot \cdot \hat{\mathbf{n}}) \\ & \times [(1 - \gamma)\hat{\mathbf{l}}_\odot + 2\gamma(\hat{\mathbf{l}}_\odot \cdot \hat{\mathbf{n}})\hat{\mathbf{n}}], \end{aligned} \quad (7)$$

where au denotes the astronomical unit, \mathcal{P}_{au} is the solar radiation pressure at 1 au from the Sun, A/m is the area-to-mass ratio of the object, $\hat{\mathbf{n}}$ is the normal to the illuminated surface, $\hat{\mathbf{l}}_\odot = (\mathbf{r}_\odot - \mathbf{r})/d_\odot$ is the Sun direction from the orbiter, and the index of reflection γ lies in the interval $(0, 1)$. Recent measurements provide the value $\mathcal{P}_{\text{au}} \approx 4.5 \cdot 10^{-6} \text{ N/m}^2$ [41].

While radiation pressure is a non-conservative effect, the acceleration it produces can be derived from a scalar function if we assume the plate is always facing the Sun. That is, $\hat{\mathbf{l}}_\odot = \hat{\mathbf{n}}$, and

$$\mathbf{a}_{\text{srp}} = -\mathcal{P}_{\text{au}} \frac{\text{au}^2}{d_\odot^2} \frac{A}{m} (1 + \gamma)\hat{\mathbf{l}}_\odot. \quad (8)$$

The radiation pressure acceleration can be recast as a fraction of solar gravity:

$$\mathbf{a}_{\text{srp}} = -\beta \mu_\odot \frac{\mathbf{r}_\odot - \mathbf{r}}{d_\odot^3}, \quad (9)$$

where

$$\beta = \frac{\mathcal{P}_{\text{au}}}{\mu_\odot} \text{au}^2 \frac{A}{m} (1 + \gamma), \quad (10)$$

is the so-called lightness number, and μ_\odot denotes the solar gravitational parameter [60]. Thus,

$$\mathbf{a}_{\text{srp}} = -\nabla_{\mathbf{r}} \mathcal{V}_{\text{srp}}, \quad (11)$$

with

$$\mathcal{V}_{\text{srp}} = \beta \frac{\mu_\odot}{d_\odot}. \quad (12)$$

In our assumption both r/d_\odot and r/r_\odot are small. Therefore, the inverse of the distance d_\odot can be written as a series expansion in Legendre polynomials:

$$\begin{aligned} \frac{r_\odot}{d_\odot} = & \frac{1}{\sqrt{1 - 2(r/r_\odot)\hat{\mathbf{r}}_\odot \cdot \hat{\mathbf{r}} + (r/r_\odot)^2}} \\ = & 1 + \frac{r}{r_\odot} \hat{\mathbf{r}}_\odot \cdot \hat{\mathbf{r}} + \sum_{i \geq 2} \frac{r^i}{r_\odot^i} P_i(\hat{\mathbf{r}}_\odot \cdot \hat{\mathbf{r}}). \end{aligned} \quad (13)$$

The constant term in the expression above does not contribute to the satellite dynamics and can be ignored. Neglecting terms $\mathcal{O}(r^2/r_\odot^2)$ and higher, we obtain the “potential”

$$\mathcal{V}_{\text{srp}} = F_{\text{srp}} \hat{\mathbf{r}}_\odot \cdot \mathbf{r}, \quad (14)$$

in which

$$F_{\text{srp}} = \beta \frac{\mu_{\odot}}{r_{\odot}^2} = \mathcal{P}_{\text{au}} \frac{\text{au}^2}{r_{\odot}^2} \frac{A}{m} (1 + \gamma) > 0. \quad (15)$$

Neglecting the eccentricity of the orbit of the Sun, $r_{\odot} = a_{\odot}$ and the true anomaly of the Sun is replaced by its longitude:

$$\lambda_{\odot} = n_{\odot} t, \quad (16)$$

where n_{\odot} is the mean motion of the Sun. Therefore, the magnitude of the acceleration F_{srp} becomes constant.

3 Hamiltonian approach

The perturbed Keplerian motion under the disturbing forces described by Eqs. (5) and (14) admits a Hamiltonian formulation. The Hamiltonian must be written in terms of a set of canonical variables. A common choice for Keplerian motion is Delaunay variables (ℓ, g, h, L, G, H) . They are usually described in terms of the standard set of Keplerian elements: semimajor axis, eccentricity, inclination, longitude of the ascending node, argument of the periaxis, and mean anomaly $(a, e, I, \Omega, \omega, M)$.

$$\begin{aligned} \ell &= M, \\ g &= \omega, \\ h &= \Omega, \\ L &= \sqrt{\mu a}, \\ G &= L\eta, \\ H &= G \cos I, \end{aligned} \quad (17)$$

where $\eta = \sqrt{1 - e^2}$.

Thus, we have a time-dependent, three-degree-of-freedom Hamiltonian

$$\mathcal{H} = \mathcal{H}(\ell, g, h, L, G, H, t) \equiv \mathcal{H}_{\text{Kepler}} + \mathcal{V}_{J_2} + \mathcal{V}_{\text{srp}}, \quad (18)$$

where

$$\mathcal{H}_{\text{Kepler}} = -\frac{\mu^2}{2L^2} = -\frac{1}{2}nL, \quad (19)$$

is the term corresponding to the restricted two-body problem, and $n = \sqrt{\mu/a^3} = \mu^2/L^3$ is the orbiter's mean motion. The explicit appearance of time in the Hamiltonian (18) originates from the longitude of the Sun in Eq. (14). Time is conveniently eliminated in a rotating frame, with angular velocity n_{\odot} , in which the first axis is aligned with the Earth-Sun direction.

In the rotating frame the definition of the Delaunay elements is unchanged except for $h = \Omega - \lambda_{\odot}$. To preserve the Hamiltonian character of the rotating frame formulation, we must include the Coriolis term

$$\mathcal{H}_{\text{Coriolis}} = -n_{\odot} \hat{\mathbf{k}}_{\odot} \cdot \mathbf{G}, \quad (20)$$

where $\hat{\mathbf{k}}_{\odot}$ is the direction of the pole of the solar orbit, and

$$\mathbf{G} = \mathbf{r} \times \frac{d\mathbf{r}}{dt} \quad (21)$$

is the specific angular momentum of the orbiter. The latter is given by $\mathbf{G} = G\hat{\mathbf{h}}$, with $\hat{\mathbf{h}}$ the unit vector in the direction of \mathbf{G} . Therefore, the Hamiltonian (18) becomes $\mathcal{K} = \mathcal{H} + \mathcal{H}_{\text{Coriolis}}$, expressed as

$$\begin{aligned} \mathcal{K} = & -\frac{1}{2}nL - n_{\odot}G\hat{\mathbf{k}}_{\odot} \cdot \hat{\mathbf{h}} \\ & + \frac{1}{2}\frac{\mu}{r}J_2\frac{a^2}{r^2}[3(\hat{\mathbf{r}} \cdot \hat{\mathbf{k}})^2 - 1] + F_{\text{srp}}\hat{\mathbf{r}}_{\odot} \cdot \mathbf{r} \end{aligned} \quad (22)$$

in vectorial form.

Assuming the effects of \mathcal{V}_{J_2} , \mathcal{V}_{srp} , and $\mathcal{H}_{\text{Coriolis}}$ are small compared to $\mathcal{H}_{\text{Kepler}}$ in Eq. (19), say $\mathcal{O}(\epsilon)$, \mathcal{K} is a perturbation Hamiltonian. Its relevant dynamical features become apparent after filtering the highest frequencies of the motion introduced by the disturbing terms.

3.1 Short-period elimination

The elimination of the high frequencies is routinely approached with the help of perturbation methods [68, 37, 22]. In our case, we apply canonical perturbation theory [73, 25]. More precisely, we rely on the Hamiltonian version of the method of Lie transforms [34, 17, 38, 33] due to its generality and versatility. It can be applied to different kinds of perturbation problems [18, 69, 49, 53], not limited to the standard case of perturbed harmonic oscillators [28, 27, 58, 48].

Thus, we remove short-period terms by means of a canonical transformation

$$\mathcal{T}_{\epsilon} : (\ell, g, h, L, G, H; \epsilon) \mapsto (\ell', g', h', L', G', H') \quad (23)$$

to prime (mean) variables, such that

$$\mathcal{T}_{\epsilon} \circ \mathcal{K} = \mathcal{K}'(-, g', h', L', G', H') + \mathcal{O}(\epsilon^2). \quad (24)$$

The transformation converting \mathcal{K} into

$$\mathcal{K}' = \langle \mathcal{K} \rangle_{\ell}(-, g', h', L', G', H'), \quad (25)$$

can be derived from the generating function

$$\mathcal{W} = \frac{1}{n} \int (\mathcal{K} - \langle \mathcal{K} \rangle_\ell) d\ell + \mathcal{O}(\epsilon^2). \quad (26)$$

More precisely, for any function of the Delaunay original variables $\xi = \xi(\ell, g, h, L, G, H)$, we can compute its transformation in terms of the prime variables $\mathcal{T}_\epsilon \circ \xi = \xi'(\ell', g', h', L', G', H')$ from

$$\xi = \xi' + \{\xi, \mathcal{W}\}. \quad (27)$$

The Poisson bracket encompassing the short-period corrections must be written in prime variables for direct corrections (27). Conversely, ξ' is written in terms of the original variables using the inverse transformation

$$\xi' = \xi - \{\xi, \mathcal{W}\}, \quad (28)$$

where the Poisson bracket is evaluated in the original, non-primed variables. Obviously, this transformation is also applicable when ξ is one of the Delaunay variables. Extensive details on the perturbation approach can be found in the original references [34, 17], or in modern textbooks such as [4, 51].

The short-period terms of Eq. (22) are revealed projecting the position vector \mathbf{r} in the apsidal frame $(\hat{\mathbf{e}}, \hat{\mathbf{b}}, \hat{\mathbf{h}})$, where $\hat{\mathbf{e}} = \mathbf{e}/e$ is the direction of the eccentricity vector

$$\mathbf{e} = \frac{1}{\mu} \frac{d\mathbf{r}}{dt} \times \mathbf{G} - \hat{\mathbf{r}}, \quad (29)$$

and $\hat{\mathbf{b}} = \hat{\mathbf{h}} \times \hat{\mathbf{e}}$. Thus,

$$\mathbf{r} = \hat{\mathbf{e}}(\mathbf{r} \cdot \hat{\mathbf{e}}) + \hat{\mathbf{b}}(\mathbf{r} \cdot \hat{\mathbf{b}}). \quad (30)$$

Using standard relations of the ellipse:

$$\begin{aligned} \mathbf{r} &= (\hat{\mathbf{e}} \cos f + \hat{\mathbf{b}} \sin f)r \\ &= [\hat{\mathbf{e}}(\cos u - e) + \hat{\mathbf{b}}\eta \sin u]a, \end{aligned} \quad (31)$$

where f and u denote the true and eccentric anomalies, and

$$r = \frac{a\eta^2}{1 + e \cos f}, \quad (32)$$

from the conic equation.

In a preliminary step, the Hamiltonian (22) is written as

$$\begin{aligned} \mathcal{K} &= -\frac{1}{2}nL - n_\odot L\eta \hat{\mathbf{k}}_\odot \cdot \hat{\mathbf{h}} + \frac{1}{3}n_* L \frac{a^2}{r^2} \frac{1}{\eta^2} \Psi(f) \\ &\quad + \frac{2}{3}n_{\text{srp}} L [(\hat{\mathbf{e}} \cdot \hat{\mathbf{r}}_\odot)(\cos u - e) + (\hat{\mathbf{b}} \cdot \hat{\mathbf{r}}_\odot)\eta \sin u], \end{aligned} \quad (33)$$

where $\mu = n^2 a^3$, $n = L/a^2$, $G = L\eta$, and

$$n_* = \frac{3}{2}nJ_2 \frac{\alpha^2}{a^2}, \quad (34)$$

$$n_{\text{srp}} = \frac{3}{2} \frac{F_{\text{srp}}}{na}, \quad (35)$$

$$\Psi \equiv [3(\hat{\mathbf{r}} \cdot \hat{\mathbf{k}})^2 - 1](1 + e \cos f). \quad (36)$$

It can be shown that

$$\begin{aligned} \Psi &= \frac{3}{2}(\hat{\mathbf{b}} \cdot \hat{\mathbf{k}})(\hat{\mathbf{e}} \cdot \hat{\mathbf{k}})(e \sin f + 2 \sin 2f + e \sin 3f) \\ &\quad - \frac{3}{4}[(\hat{\mathbf{b}} \cdot \hat{\mathbf{k}})^2 - (\hat{\mathbf{e}} \cdot \hat{\mathbf{k}})^2](e \cos 3f + 2 \cos 2f) \\ &\quad + \frac{1}{4}[3(\hat{\mathbf{b}} \cdot \hat{\mathbf{k}})^2 + 9(\hat{\mathbf{e}} \cdot \hat{\mathbf{k}})^2 - 4]e \cos f \\ &\quad + \frac{1}{2}[3(\hat{\mathbf{b}} \cdot \hat{\mathbf{k}})^2 + 3(\hat{\mathbf{e}} \cdot \hat{\mathbf{k}})^2 - 2]. \end{aligned} \quad (37)$$

The average of the Hamiltonian (33) over the mean anomaly is obtained in closed form using the basic differential relations of Keplerian motion

$$d\ell = \frac{r}{a} du = \left(\frac{r}{a}\right)^2 \frac{1}{\eta} df. \quad (38)$$

Substituting the expressions $r/a = 1 - e \cos u$ and $r/a = \eta^2/(1 + e \cos f)$, we obtain

$$\begin{aligned} \langle \mathcal{K} \rangle_\ell &= -\frac{L}{2}n - n_\odot L\eta \hat{\mathbf{k}}_\odot \cdot \hat{\mathbf{h}} - Ln_{\text{srp}} \hat{\mathbf{r}}_\odot \cdot \mathbf{e} \\ &\quad + \frac{L}{6\eta^3} n_* [3(\hat{\mathbf{b}} \cdot \hat{\mathbf{k}})^2 + 3(\hat{\mathbf{e}} \cdot \hat{\mathbf{k}})^2 - 2]. \end{aligned} \quad (39)$$

The generating function of the short-period elimination is computed from Eq. (26):

$$\begin{aligned} \mathcal{W} &= \frac{L}{12\eta^3} \frac{n_*}{n} \left\{ [6(\hat{\mathbf{b}} \cdot \hat{\mathbf{k}})^2 + 6(\hat{\mathbf{e}} \cdot \hat{\mathbf{k}})^2 - 4](f - \ell) \right. \\ &\quad + [3(\hat{\mathbf{b}} \cdot \hat{\mathbf{k}})^2 + 9(\hat{\mathbf{e}} \cdot \hat{\mathbf{k}})^2 - 4]e \sin f \\ &\quad - [(\hat{\mathbf{b}} \cdot \hat{\mathbf{k}})^2 - (\hat{\mathbf{e}} \cdot \hat{\mathbf{k}})^2](e \sin 3f + 3 \sin 2f) \\ &\quad + 2(\hat{\mathbf{b}} \cdot \hat{\mathbf{k}})(\hat{\mathbf{e}} \cdot \hat{\mathbf{k}})(3e \cos f + 3 \cos 2f + e \cos 3f) \left. \right\} \\ &\quad + \frac{n_{\text{srp}} L}{n} \frac{1}{6} \left\{ [2(2 - e^2) \sin u - e \sin 2u] \hat{\mathbf{e}} \cdot \hat{\mathbf{r}}_\odot \right. \\ &\quad \left. - \eta(4 \cos u - e \cos 2u) \hat{\mathbf{b}} \cdot \hat{\mathbf{r}}_\odot \right\} + \mathcal{C}, \end{aligned} \quad (40)$$

where $\mathcal{C} \equiv \mathcal{C}(-, g, h, L, G, H)$ is an arbitrary function arising from the quadrature in Eq. (26). While any choice of \mathcal{C} would be valid from the point of view of the perturbation approach, it is common practice to select a \mathcal{W} that only includes short-period terms. That is, $\langle \mathcal{W} \rangle_\ell = 0$, in which case we determine $\mathcal{C} = \langle \mathcal{C} - \mathcal{W} \rangle_\ell$ from Eq. (40). Using known primitives from the literature [43, 40], we obtain

$$\mathcal{C} = \frac{L n_* e^2}{6 n \eta^3} \frac{1 + 2\eta}{(1 + \eta)^2} (\hat{\mathbf{b}} \cdot \hat{\mathbf{k}})(\hat{\mathbf{e}} \cdot \hat{\mathbf{k}}) - \frac{n_{\text{srp}} L}{n} \frac{e\eta \hat{\mathbf{b}} \cdot \hat{\mathbf{r}}_\odot}{3}.$$

The transformations from mean to osculating variables and viceversa, given in Eqs. (27) and (28), are then computed evaluating Poisson brackets.

Finally, original variables are replaced with mean values in Eq. (39) to obtain the transformed Hamiltonian \mathcal{K}' (25). This requires evaluating the frequencies n_* and n_{srp} (Eqs. (34) and (35)) in prime variables. After neglecting higher-order terms, ℓ' becomes cyclic. In consequence, L' , $a = a(L')$, and the frequencies n_* and n_{srp} are integrals of the truncated Hamiltonian in the new variables.

3.2 Long-term dynamics

The long-term dynamics can be studied after neglecting the constant Keplerian term in Eq. (39):

$$\mathcal{K}' = -L' n_\odot \eta \hat{\mathbf{k}}_\odot \cdot \hat{\mathbf{h}} - L' n_{\text{srp}} e \hat{\mathbf{r}}_\odot \cdot \hat{\mathbf{e}} - \frac{L' n_*}{6\eta^3} [3(\hat{\mathbf{h}} \cdot \hat{\mathbf{k}})^2 - 1], \quad (41)$$

where all terms are expressed using the prime Delaunay variables, and we substituted the identity

$$(\hat{\mathbf{e}} \cdot \hat{\mathbf{k}})^2 + (\hat{\mathbf{b}} \cdot \hat{\mathbf{k}})^2 + (\hat{\mathbf{h}} \cdot \hat{\mathbf{k}})^2 = 1. \quad (42)$$

The long-term dynamics are obtained from the numerical integration of the Hamilton equations. Denoting

$$\boldsymbol{\eta} = \eta \hat{\mathbf{h}} = \mathbf{G}/L', \quad (43)$$

the flow of the Hamiltonian (41) can be written in dimensionless, non-canonical, symmetric form

$$\frac{d\boldsymbol{\eta}}{dt} = n_\odot \boldsymbol{\eta} \times \hat{\mathbf{k}}_\odot + n_{\text{srp}} \mathbf{e} \times \hat{\mathbf{r}}_\odot + \frac{n_*}{\eta^5} (\boldsymbol{\eta} \cdot \hat{\mathbf{k}}) \boldsymbol{\eta} \times \hat{\mathbf{k}}, \quad (44)$$

$$\frac{d\mathbf{e}}{dt} = n_\odot \mathbf{e} \times \hat{\mathbf{k}}_\odot + n_{\text{srp}} \boldsymbol{\eta} \times \hat{\mathbf{r}}_\odot + \frac{n_*}{\eta^5} (\boldsymbol{\eta} \cdot \hat{\mathbf{k}}) \mathbf{e} \times \hat{\mathbf{k}} + \frac{n_*}{2\eta^5} \left[1 - \frac{5}{\eta^2} (\boldsymbol{\eta} \cdot \hat{\mathbf{k}})^2 \right] \mathbf{e} \times \boldsymbol{\eta}. \quad (45)$$

These differential equations are redundant due to the orthogonality of \mathbf{e} and $\boldsymbol{\eta}$. The symmetric character of the vectorial formulation allows for an efficient implementation in software, as reported in [55, 76]. Retaining only first-order effects, Eqs. (44)–(45) can be obtained adding the first terms of the mean variations of the gravitational potential to those of the problem with radiation pressure only. See Eqs. (29)–(30) in [76] and Eqs. (9.8)–(9.9) in [51].

The differential system Eqs. (44)–(45) approximates the averaged dynamics when the three frequencies n_\odot , n_* , and n_{srp} are of comparable magnitude—as required by the perturbation approach. Situations where this assumption applies have been discussed in the literature. As an example, an object with area-to-mass ratio $A/m = 408 \text{ cm}^2/\text{gr}$ describing an elliptical path with a semimajor axis of 17800 km around the Earth has $n_\odot = n_*/0.275 = n_{\text{srp}}/0.295$. See Table 2 of [45] where $C \equiv n_{\text{srp}}/n_\odot$ and $W \equiv n_*/n_\odot$.

4 The coplanar manifold

While no closed-form integral of the Hamiltonian flow (41) is available, there is a coplanar invariant manifold. If we neglect the axial tilt of the planet, i.e. $\hat{\mathbf{k}} = \hat{\mathbf{k}}_\odot$, equatorial orbits do not experience changes in inclination. If the spacecraft starts in an equatorial orbit, the variation of $\boldsymbol{\eta}$ given by Eq. (44) has the direction of $\boldsymbol{\eta}$, and the motion is constrained to the plane of the equator.

We can study this particular invariant manifold by setting $\hat{\mathbf{k}}_\odot \cdot \hat{\mathbf{h}} = \hat{\mathbf{h}} \cdot \hat{\mathbf{k}} = 1$ and $\hat{\mathbf{r}}_\odot \cdot \hat{\mathbf{e}} = \cos \theta$ in Eq. (41). The polar angle θ formed by the directions of the Sun and the orbit periapsis³ is the conjugate coordinate to the specific angular momentum $\Theta = G'$. Then,

$$\mathcal{K}_{\text{coplanar}} = -L' \left(n_\odot \eta + \frac{n_*}{3\eta^3} + n_{\text{srp}} e \cos \theta \right). \quad (46)$$

Recall that $\eta = \Theta/L'$ from Eq. (17).

4.1 Equilibria

Note that the rates of change of θ and Θ

$$\frac{d\theta}{dt} = \frac{\partial \mathcal{K}_{\text{coplanar}}}{\partial \Theta} = \frac{n_*}{\eta^4} - n_\odot + n_{\text{srp}} \frac{\eta}{e} \cos \theta, \quad (47)$$

$$\frac{d\Theta}{dt} = -\frac{\partial \mathcal{K}_{\text{coplanar}}}{\partial \theta} = -n_{\text{srp}} L' e \sin \theta, \quad (48)$$

vanish when $\theta = 0$ or $\theta = \pi$, and

³ Some authors use the supplementary angle of θ .

$$(n_* - n_{\odot}\eta^4)e \pm n_{\text{srp}}\eta^5 = 0, \quad (49)$$

where the sign depends on the value of θ . Equation (49) can be recast into

$$(n_* - n_{\odot}\eta^4)^2 e^2 - n_{\text{srp}}^2 \eta^{10} = 0, \quad (50)$$

which is always valid and is a quintic polynomial in η^2 . Replacing $e^2 = 1 - \eta^2$ and expanding the factors gives

$$(\tilde{n}_{\text{srp}}^2 + 1)\eta^{10} - \eta^8 - 2\tilde{n}_*\eta^6 + 2\tilde{n}_*\eta^4 + \tilde{n}_*^2\eta^2 - \tilde{n}_*^2 = 0, \quad (51)$$

in which the radiation pressure parameter

$$\tilde{n}_{\text{srp}} = \frac{n_{\text{srp}}}{n_{\odot}} \quad (52)$$

increases with the area-to-mass ratio. The oblateness parameter

$$\tilde{n}_* = \frac{n_*}{n_{\odot}} \quad (53)$$

decreases when the semi-major axis grows. From Descartes' rule of signs, Eq. (51) has either 3 or 1 real roots, corresponding to eccentricity values for which the periapsis remains frozen. In general, the roots of Eq. (51) must be computed numerically from given values of \tilde{n}_{srp} and \tilde{n}_* . However, because the resultant of the quintic polynomial and its derivative with respect to η must vanish for multiple roots, we succeeded in computing analytically the bifurcation line $\tilde{n}_{\text{srp}} = \tilde{n}_{\text{srp}}(\tilde{n}_*)$ that separates the regions of the parameters plane admitting one or three equilibria. We first compute the discriminant Δ of Eq. (51):

$$\Delta = 1024[3125\tilde{n}_*\tilde{n}_{\text{srp}}^4 + 32\tilde{n}_*(8\tilde{n}_*^2 - 25\tilde{n}_* + 125)\tilde{n}_{\text{srp}}^2 + 256(\tilde{n}_* - 1)^3]^2 \tilde{n}_*^{16} \tilde{n}_{\text{srp}}^8 (\tilde{n}_{\text{srp}}^2 + 1). \quad (54)$$

Disregarding the degenerate cases $\tilde{n}_* = 0$ and $\tilde{n}_{\text{srp}} = 0$, setting the discriminant to zero yields a biquadratic polynomial in \tilde{n}_{srp} , whose coefficients are polynomials in \tilde{n}_* . Solving for \tilde{n}_{srp} gives

$$\tilde{n}_{\text{srp}} = \frac{4\sqrt{5}}{125}\tilde{n}_*\sqrt{\frac{5 - \tilde{n}_*}{\tilde{n}_*}\left[\left(4 + \frac{5}{\tilde{n}_*}\right)^{\frac{3}{2}} - \frac{25}{\tilde{n}_*}\right]} - 8. \quad (55)$$

The bifurcation line given by Eq. (55) is represented in the parameters plane $\tilde{n}_* - \tilde{n}_{\text{srp}}$ with a black curve in Fig. 2. Below this line, there are always three equilibria (shaded area of Fig. 2). Two of them merge at the bifurcation line and cease to exist above it (light area of Fig. 2), where just one remains. We will show later that this bifurcation line is of the saddle-node type. Because the line only exists in the interval $0 < \tilde{n}_* \leq 1$, there is only one fixed point when $n_* > n_{\odot}$.

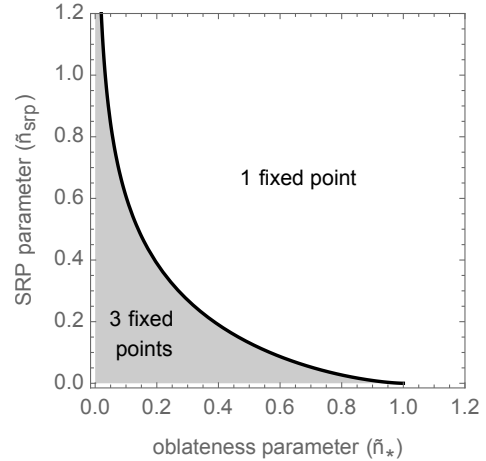


Fig. 2 Regions of the parameters plane with different numbers of fixed points (shaded and white areas) of the coplanar flow.

4.2 Changes of local nature of the reduced flow

For a given point $(\tilde{n}_*, \tilde{n}_{\text{srp}})$ of the parameters plane, the reduced flow can be visualized without integrating Eqs. (47)–(48) by plotting contours of the Hamiltonian (scaled by $L'n_{\odot}$) in eccentricity vector diagrams:

$$\mathcal{K}' = -\eta - \frac{\tilde{n}_*}{3\eta^3} - \tilde{n}_{\text{srp}}e \cos \theta. \quad (56)$$

The reduced flow in the region above the bifurcation line (light area of Fig. 2) is shown in Fig. 3 for decreasing values of \tilde{n}_* and a constant value $\tilde{n}_{\text{srp}} = 3^{-1/2}$. The latter has been chosen because it represents a typical case for moderate radiation pressure perturbations, see [63]. For clarity, the phase plots are depicted in both eccentricity vector representation $(e \cos \theta, e \sin \theta)$ and cylindrical map form (θ, e) . Dotted contours in Fig. 3 correspond to the manifold

$$\mathcal{K}'_0 = -1 - \frac{1}{3}\tilde{n}_*, \quad (57)$$

of orbits that become temporarily circular, obtained making $e = 0$, and hence $\eta = 1$ in Eq. (56). The top plots of Fig. 3 illustrated a situation far from the bifurcation. We observe an interior region of orbits where the periapsis oscillates around the elliptic fixed point with $\theta = \pi$, and an exterior region with rotating periapsis. They are separated by the dotted contour of the \mathcal{K}'_0 manifold. As shown in the middle section of Fig. 3, the interior region of orbits with oscillating periapsis becomes larger when approaching the bifurcation line, while the flow bends towards the axis of abscissas. When the saddle-node bifurcation occurs (bottom pane of Fig. 3) a cusp appears on the symmetry axis.

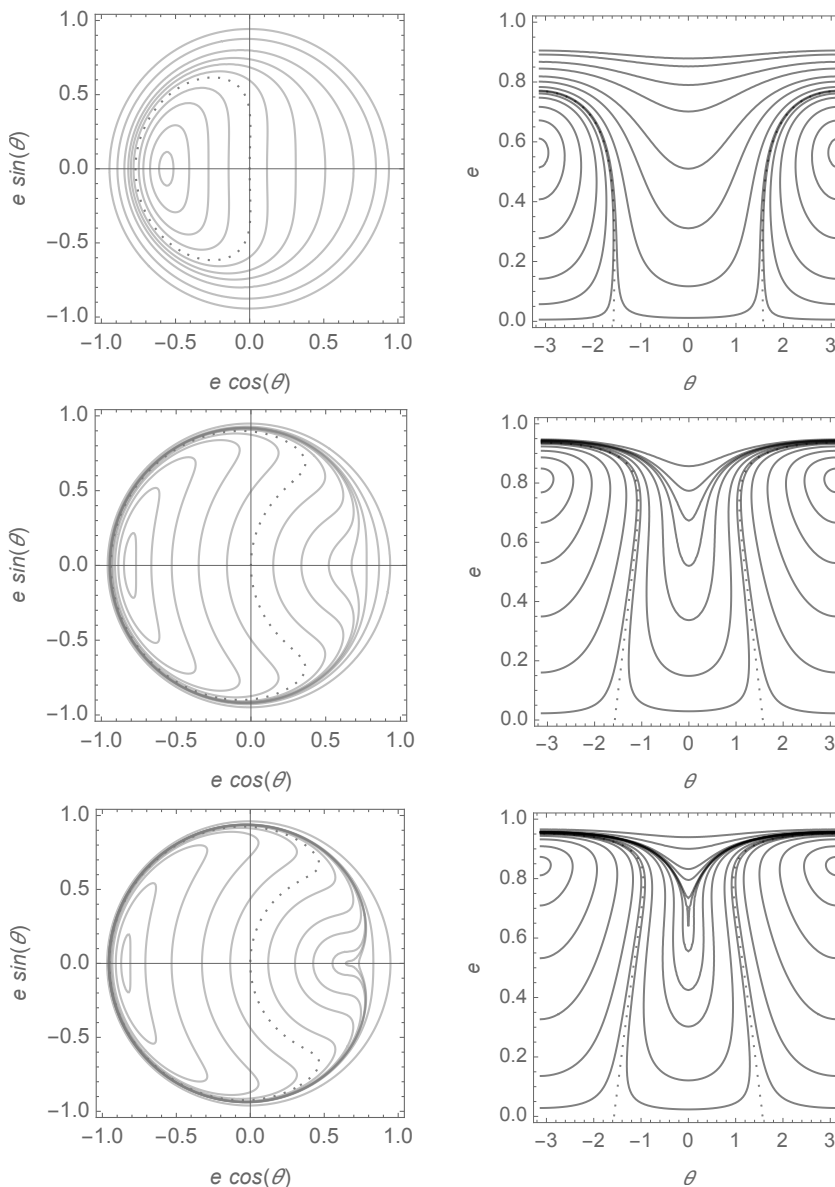


Fig. 3 Coplanar orbits for $\tilde{n}_{\text{srp}} = 3^{-1/2}$ and $\tilde{n}_* = 0.85$ (top), 0.16 (center) and 0.11 (bottom). Dotted contours mark transitions between rotation and oscillation of the eccentricity vector.

Below the bifurcation line (shaded area of Fig. 2) we find two additional fixed points, one elliptic and one hyperbolic, both with periapsis at $\theta = 0$. The energy manifold \mathcal{K}'_{U} of the hyperbolic fixed point plays a fundamental role in the qualitative changes experienced by the flow. As shown in the top plots of Fig. 4, an additional region of orbits with oscillating periapsis exists centered on the elliptic fixed point with $\theta = 0$. It is bounded by the dashed contour corresponding to \mathcal{K}'_{U} , which splits the orbits with rotating periapsis in two subsets: one between \mathcal{K}'_0 and \mathcal{K}'_{U} , and the other, which is made of highly eccentric orbits, bounded by the exterior branch of \mathcal{K}'_{U} .

4.3 Global changes of the flow

There are points of the parameters plane where \mathcal{K}'_0 may overlap to \mathcal{K}'_{U} , as illustrated in the center section of Fig. 4. When this occurs, the interior region of orbits with circulating periapsis surrounding the elliptic fixed point with $\theta = \pi$ collapses to the curve defined by the interior branch of \mathcal{K}'_{U} , ceasing to exist. Only three regions with different flow remain: an exterior area made of highly eccentric orbits with circulating periapsis and two interior regions with the periapsis oscillating around an elliptic fixed point.

The critical condition $\mathcal{K}'_0 = \mathcal{K}'_{\text{U}}$ is expressed as a function of η from Eqs. (56) and (57):

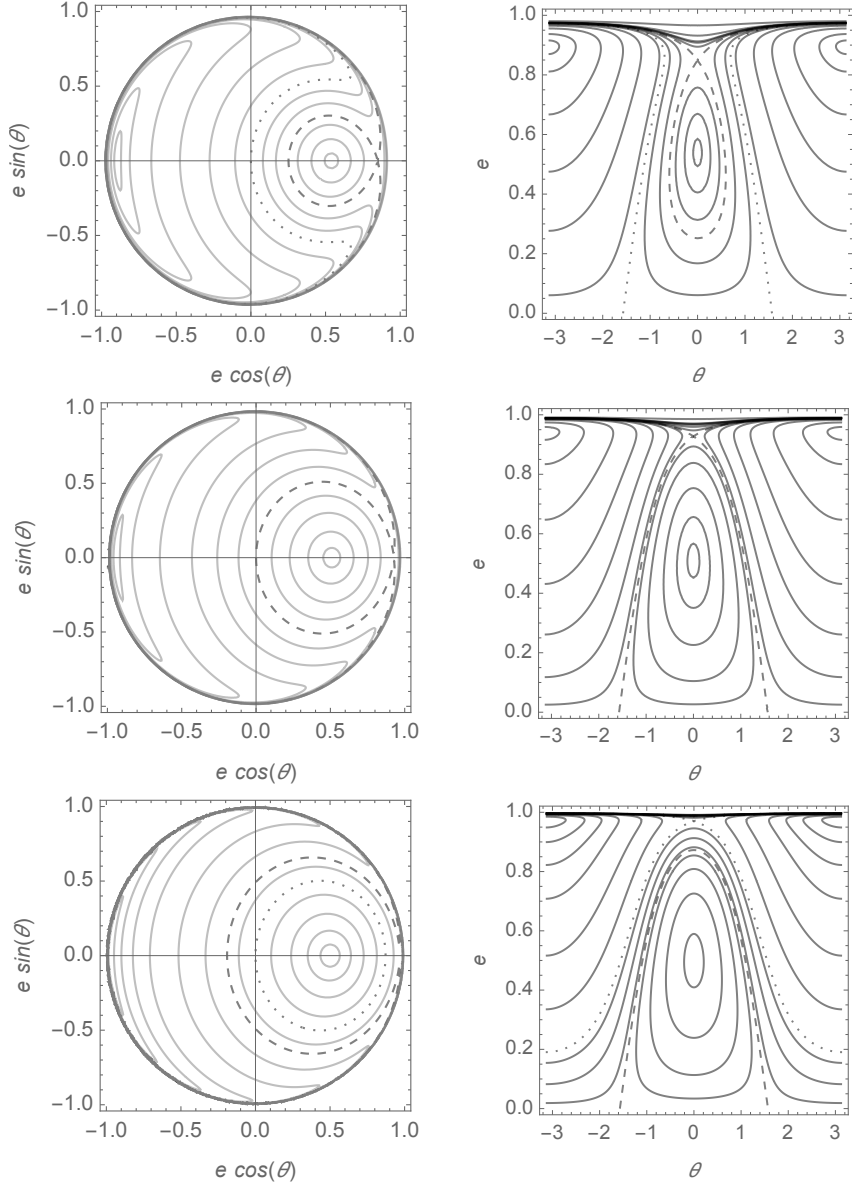


Fig. 4 Coplanar orbits for $\tilde{n}_{\text{srp}} = 3^{-1/2}$ and $\tilde{n}_* = 0.05$ (top), 0.015 (center), and 0.003 (bottom). Dashed contour is the energy manifold of the hyperbolic fixed point, dotted lines ones separate regions with rotating and oscillating periapsis.

$$1 + \frac{1}{3}\tilde{n}_* = \tilde{n}_{\text{srp}}e + \eta + \frac{1}{3}\frac{\tilde{n}_*}{\eta^3}. \quad (58)$$

Substituting $e = \sqrt{1 - \eta^2}$ yields a polynomial equation in η ,

$$0 = 9(\tilde{n}_{\text{srp}}^2 + 1)\eta^7 + (9\tilde{n}_{\text{srp}}^2 - 9 - 6\tilde{n}_*)\eta^6 + \tilde{n}_*^2\eta^5 + \tilde{n}_*^2\eta^4 + \tilde{n}_*(\tilde{n}_* + 6)\eta^3 - \tilde{n}_*^2\eta^2 - \tilde{n}_*^2\eta - \tilde{n}_*^2, \quad (59)$$

which may admit either one or three real roots according to Descartes' rule. In particular, only one real root is possible if $\tilde{n}_* \leq \frac{3}{2}(\tilde{n}_{\text{srp}}^2 - 1)$, the condition that ensures the coefficient of η^6 in Eq. (59) is non-negative.

Therefore, the value of η that makes $\mathcal{K}'_{\text{U}} = \mathcal{K}'_0$ must be a common root of Eqs. (59) and (51). From the resultant of the corresponding polynomials, we obtain the critical line $\tilde{n}_{\text{srp}} = \tilde{n}_{\text{srp}}(\tilde{n}_*)$ in implicit form

$$0 = 59049\tilde{n}_{\text{srp}}^8 - 243\tilde{n}_{\text{srp}}^6(647\tilde{n}_*^2 + 2538\tilde{n}_* + 972) - 2\tilde{n}_{\text{srp}}^4(1603\tilde{n}_*^4 - 13500\tilde{n}_*^3 + 49572\tilde{n}_*^2 + 291600\tilde{n}_* - 177147) + 6\tilde{n}_{\text{srp}}^2(25\tilde{n}_*^6 - 205\tilde{n}_*^5 - 6604\tilde{n}_*^4 - 35714\tilde{n}_*^3 - 140967\tilde{n}_*^2 - 274833\tilde{n}_* - 39366) - 3(\tilde{n}_* - 1)^3(\tilde{n}_* + 3)(\tilde{n}_*^2 + 14\tilde{n}_* + 81)^2. \quad (60)$$

The solution $\tilde{n}_{\text{srp}} = \tilde{n}_{\text{srp}}(\tilde{n}_*)$ of Eq. (60) is represented in Fig. 5 with a dashed curve.

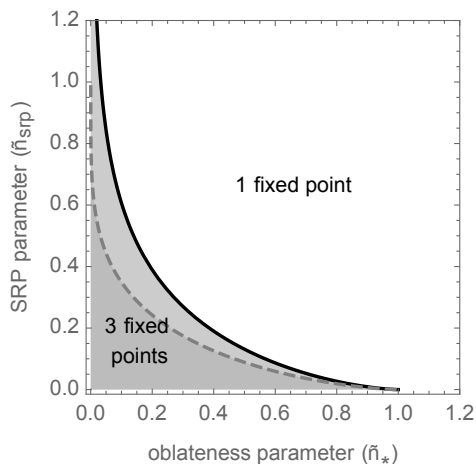


Fig. 5 Regions of the parameters plane of the coplanar flow with different qualitative behavior.

After crossing the critical line a region of orbits with rotating periapsis around the elliptic fixed point with $\theta = 0$ develops between the manifolds \mathcal{K}'_0 and \mathcal{K}'_U (bottom section of Fig. 4). This is in stark contrast with the situation before the crossing (top pane of the figure) where the orbits contained between these two manifolds revolve around the $\theta = \pi$ elliptic point. Thus, the line defined by Eq. (60) marks a global transition in the flow, as opposed to the local nature of the bifurcation boundary given by Eq. (55).

4.4 The reduced flow on the sphere

In the graphics of the previous section, the behavior of the highest eccentricity orbits is difficult to appreciate. A sphere provides better visualization [47, 19, 15, 12, 48]. Introducing the variables

$$\chi_1 = e\eta \cos g, \quad (61)$$

$$\chi_2 = e\eta \sin g, \quad (62)$$

$$\chi_3 = \eta^2 - \frac{1}{2}, \quad (63)$$

the Hamiltonian (56) can be rewritten as

$$\mathcal{K}' = -\eta - \frac{\tilde{n}_*}{3\eta^3} - \tilde{n}_{\text{srp}} \frac{\chi_1}{\eta}. \quad (64)$$

In Eq. (63), η can be expressed in terms of χ_3 : $\eta = \sqrt{\frac{1}{2} + \chi_3}$. The flow corresponds to the intersection of the manifold $\mathcal{K}'(\chi_1, -, \chi_3) = \kappa < 0$ (64) with the sphere

$$\chi_1^2 + \chi_2^2 + \chi_3^2 = \frac{1}{4}, \quad (65)$$

of radius $\frac{1}{2}$. Circular orbits ($e = 0$, $\eta = 1$) lie on the north pole of the sphere $(0, 0, \frac{1}{2})$, whereas the orbits with the maximum eccentricity ($e \rightarrow 1$, $\eta \rightarrow 0$) collapse to the south pole $(0, 0, -\frac{1}{2})$.

For a given energy κ , a trajectory on the sphere is computed as a sequence of points. First, we choose a value of χ_3 in the interval $]-\frac{1}{2}, \frac{1}{2}]$. Next, we solve $\chi_1 = \chi_1(\chi_3; \kappa)$ from Eq. (64) to obtain

$$\chi_1 = -\frac{1}{\tilde{n}_{\text{srp}}} \left(\eta^2 + \kappa\eta + \frac{1}{3} \frac{\tilde{n}_*}{\eta^2} \right), \quad (66)$$

where $\eta \equiv \eta(\chi_3)$. Finally, we compute χ_2 from Eq. (65):

$$\chi_2 = \pm \left(\frac{1}{4} - \chi_1^2 - \chi_3^2 \right)^{\frac{1}{2}}.$$

The case $\tilde{n}_{\text{srp}} = 3^{-1/2}$, $\tilde{n}_* = 0.05$, previously presented in the first row of Fig. 4, is shown in Fig. 6. It highlights the circulation of highly elliptic orbits around the south pole of the sphere.

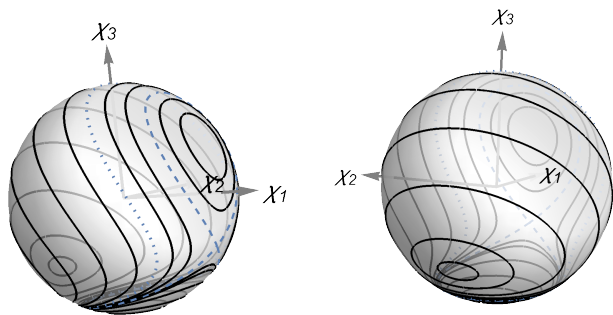


Fig. 6 Different views of the reduced coplanar flow on the sphere for $\tilde{n}_{\text{srp}} = 3^{-1/2}$, $\tilde{n}_* = 0.05$, corresponding to the first row of Fig. 4.

5 Conclusions

The long term behavior of a high area-to-mass ratio object orbiting a planet may undergo important qualitative changes induced by the oblateness perturbation of the central body. Moving beyond resonant cases, extensively discussed in the literature due to their interest for astrodynamics applications, we focused on coplanar orbits. Neglecting the axial tilt of the planet, the equatorial orbits of this kind of objects constitute an invariant manifold of the oblate-solar radiation pressure problem, integrable up to higher-order effects. The invariance of the coplanar manifold is evidenced by the vectorial formulation presented. The generality of the

approach, based on the fundamental vectors defining the apsidal frame, and free from singularities, may offer advantages for semi-analytical integration.

Particular cases of the solution presented in this contribution can be found in the literature. We generalised the treatment using a rigorous and formal approach. We derived the generating function of the transformation for the averaging explicitly. We selected the arbitrary function on which the mean-to-osculating transformation depends to ensure the latter is purely periodic. This is a prerequisite for extending the theory to second order. We extended the existing literature by thoroughly exploring the qualitative behavior of the coplanar manifold in a two-parameter plane. One of the parameters is related to the physical characteristics of the orbiter, while the other is associated with the dynamical characteristics of the orbit. We computed analytically two critical boundaries delimiting three regions with different qualitative flow. The characteristics of the flow depend on the balance between the solar radiation pressure and the oblateness perturbations. Local changes to the flow appear in the form of bifurcations of orbits with the periapsis frozen in the radiation pressure direction. Global variations in the flow are possible. Orbits with rotating periapsis can switch from circling the fixed point with periapsis towards the Sun, to revolving around the opposite frozen orbit.

Acknowledgements The authors acknowledge Khalifa University of Science and Technology's internal grant CIRA-2021-65 (8474000413). ML also acknowledges partial support from the Spanish State Research Agency and the European Regional Development Fund (Projects PID2020-112576GB-C22 and PID2021-123219OB-I00, AEI/ERDF, EU). EF has been partially supported by Spanish MINECO's funds PID2020-112576GB-C21 and PID2021-1239 68NB-I00. RF received support from MINECO "Severo Ochoa Programme for Centres of Excellence in R&D" (CEX2018-000797-S).

Conflict of interest

The authors declare that they have no conflict of interest.

Authors contributions

The study conception and design were performed by M. Lara who wrote the first draft of the manuscript. All authors collaborated on improving subsequent versions of the paper, and read and approved the final manuscript.

Funding

The financial support for the execution of the research here presented was provided by the following grants: Khalifa University of Science and Technology's CIRA-2021-65 / 8474000413 (recipient: E. Fantino), Spanish National funds PID2020-112576GB-C22 (recipient: M. Lara), PID2021-123219OB-I00 (recipient: M. Lara), PID2020-112576GB-C21 (recipient: E. Fantino), PID2021-123968NB-I00 (recipient: E. Fantino) and CEX2018-000797-S (recipient: R. Flores).

Data availability

No datasets, other than the numerical results presented in the figures, have been generated as part of this research. The information provided in this manuscript is sufficient to reproduce those results.

References

1. Aksnes, K.: Short-period and long-period perturbations of a spherical satellite due to direct solar radiation. *Celestial Mechanics* **13**, 89–104 (1976). DOI 10.1007/BF01228536
2. Alessi, E.M., Colombo, C., Rossi, A.: Phase space description of the dynamics due to the coupled effect of the planetary oblateness and the solar radiation pressure perturbations. *Celestial Mechanics and Dynamical Astronomy* **131**(9), 43 (2019). DOI 10.1007/s10569-019-9919-z
3. Arnold, V.I.: *Mathematical Methods of Classical Mechanics*, *Graduate Texts in Mathematics*, vol. 60, 2nd edn. Springer-Verlag, New York (1989). DOI 10.1007/978-1-4757-2063-1
4. Boccaletti, D., Pucacco, G.: *Theory of orbits. Volume 2: Perturbative and geometrical methods*, 1st edn. *Astronomy and Astrophysics Library*. Springer-Verlag, Berlin Heidelberg New York (2002)
5. Breakwell, J.V., Vagners, J.: On Error Bounds and Initialization in Satellite Orbit Theories. *Celestial Mechanics* **2**, 253–264 (1970). DOI 10.1007/BF01229499
6. Brouwer, D.: Solution of the problem of artificial satellite theory without drag. *The Astronomical Journal* **64**, 378–397 (1959). DOI 10.1086/107958
7. Brouwer, D.: Analytical study of resonance caused by solar radiation pressure. In: M. Roy (ed.) *Dynamics of Satellites / Dynamique des Satellites*, IUTAM Symposia (International Union of Theoretical and Applied Mechanics), pp. 34–39. Springer, Berlin, Heidelberg (1963). DOI 10.1007/978-3-642-48130-7_4
8. Burns, J.A., Lamy, P.L., Soter, S.: Radiation forces on small particles in the solar system. *Icarus* **40**(1), 1–48 (1979). DOI 10.1016/0019-1035(79)90050-2
9. Cain, B.J.: Determination of mean elements for Brouwer's satellite theory. *Astronomical Journal* **67**, 391–392 (1962). DOI 10.1086/108745
10. Chamberlain, J.W., Bishop, J.: Radiation pressure dynamics in planetary exospheres. II - Closed solutions for the evolution of orbital elements. *Icarus* **106**, 419–427 (1993). DOI 10.1006/icar.1993.1182
11. Coffey, S.L., Deprit, A.: Third-Order Solution to the Main Problem in Satellite Theory. *Journal of Guidance, Control and Dynamics* **5**(4), 366–371 (1982). DOI 10.2514/3.56183

12. Coffey, S.L., Deprit, A., Miller, B.R.: The critical inclination in artificial satellite theory. *Celestial Mechanics* **39**(4), 365–406 (1986). DOI 10.1007/BF01230483
13. Colombo, C., Lücking, C., McInnes, C.R.: Orbital dynamics of high area-to-mass ratio spacecraft with J_2 and solar radiation pressure for novel Earth observation and communication services. *Acta Astronautica* **81**(1), 137–150 (2012). DOI <https://doi.org/10.1016/j.actaastro.2012.07.009>
14. Cook, G.E.: Luni-Solar Perturbations of the Orbit of an Earth Satellite. *Geophysical Journal* **6**, 271–291 (1962). DOI 10.1111/j.1365-246X.1962.tb00351.x
15. Cushman, R.: Reduction, Brouwer's Hamiltonian, and the critical inclination. *Celestial Mechanics* **31**(4), 401–429 (1983). DOI 10.1007/BF01230294
16. Danby, J.M.A.: *Fundamentals of Celestial Mechanics*. Willmann-Bell, Richmond, VA (1992)
17. Deprit, A.: Canonical transformations depending on a small parameter. *Celestial Mechanics* **1**(1), 12–30 (1969). DOI 10.1007/BF01230629
18. Deprit, A.: The elimination of the parallax in satellite theory. *Celestial Mechanics* **24**(2), 111–153 (1981). DOI 10.1007/BF01229192
19. Deprit, A.: The reduction to the rotation for planar perturbed Keplerian systems. *Celestial Mechanics* **29**, 229–247 (1983). DOI 10.1007/BF01229137
20. Deprit, A.: Dynamics of orbiting dust under radiation pressure. In: A. Berger (ed.) *The Big-Bang and Georges Lemaître*, pp. 151–180. Springer, Dordrecht (1984). DOI 10.1007/978-94-009-6487-7_14
21. Deprit, A., Rom, A.: The Main Problem of Artificial Satellite Theory for Small and Moderate Eccentricities. *Celestial Mechanics* **2**(2), 166–206 (1970). DOI 10.1007/BF01229494
22. Di Nino, S., Luongo, A.: Nonlinear dynamics of a base-isolated beam under turbulent wind flow. *Nonlinear Dynamics* **107**(2), 1529–1544 (2022). DOI 10.1007/s11071-021-06412-4
23. Feng, J., Hou, X.Y.: Secular dynamics around small bodies with solar radiation pressure. *Communications in Nonlinear Science and Numerical Simulations* **76**, 71–91 (2019). DOI 10.1016/j.cnsns.2019.02.011
24. Ferraz Mello, S.: Analytical Study of the Earth's Shadowing Effects on Satellite Orbits. *Celestial Mechanics* **5**, 80–101 (1972). DOI 10.1007/BF01227825
25. Ferraz-Mello, S.: *Canonical Perturbation Theories - Degenerate Systems and Resonance*, *Astrophysics and Space Science Library*, vol. 345. Springer, New York (2007)
26. Ferrer, S., Lara, M.: Integration of the Rotation of an Earth-like Body as a Perturbed Spherical Rotor. *The Astronomical Journal* **139**(5), 1899–1908 (2010). DOI 10.1088/0004-6256/139/5/1899
27. Ferrer, S., Lara, M., Palacián, J., Juan, J.F.S., Viartola, A., Yanguas, P.: The Hénon and Heiles Problem in Three Dimensions. II. Relative equilibria and bifurcations in the reduced system. *International Journal of Bifurcation and Chaos* **08**(6), 1215–1229 (1998). DOI 10.1142/s0218127498000954
28. Giorgilli, A., Galgani, L.: Formal integrals for an autonomous Hamiltonian system near an equilibrium point. *Celestial Mechanics* **17**, 267–280 (1978). DOI 10.1007/BF01232832
29. Gkolias, I., Alessi, E.M., Colombo, C.: Dynamical taxonomy of the coupled solar radiation pressure and oblateness problem and analytical deorbiting configurations. *Celestial Mechanics and Dynamical Astronomy* **132**(11), 55 (2020). DOI 10.1007/s10569-020-09992-2
30. Hamilton, D.P.: Motion of Dust in a Planetary Magnetosphere: Orbit-Averaged Equations for Oblateness, Electromagnetic, and Radiation Forces with Application to Saturn's E Ring. *Icarus* **101**(2), 244–264 (1993). DOI 10.1006/icar.1993.1022
31. Hamilton, D.P., Krivov, A.V.: Circumplanetary Dust Dynamics: Effects of Solar Gravity, Radiation Pressure, Planetary Oblateness, and Electromagnetism. *Icarus* **123**(2), 503–523 (1996). DOI 10.1006/icar.1996.0175
32. Heiligers, J., Fernandez, J.M., Stohlman, O.R., Wilkie, W.K.: Trajectory design for a solar-sail mission to asteroid 2016 HO₃. *Astrodynamics* **3**(3), 231–246 (2019). DOI 10.1007/s42064-019-0061-1
33. Henrard, J.: On a perturbation theory using Lie transforms. *Celestial Mechanics* **3**, 107–120 (1970). DOI 10.1007/BF01230436
34. Hori, G.i.: *Theory of General Perturbation with Unspecified Canonical Variables*. Publications of the Astronomical Society of Japan **18**(4), 287–296 (1966)
35. Hughes, S.: Satellite orbits perturbed by direct solar radiation pressure - General expansion of the disturbing function. *Planetary and Space Science* **25**, 809–815 (1977). DOI 10.1016/0032-0633(77)90034-4
36. Jastrow, R., Bryant, R.: Variations in the Orbit of the Echo Satellite. *Journal of Geophysical Research* **65**, 3512 (1960). DOI 10.1029/JZ065i010p03512
37. Kahn, P.B., Zarmi, Y.: Nonlinear dynamics: A tutorial on the method of normal forms. *American Journal of Physics* **68**(10), 907–919 (2000). DOI 10.1119/1.1285895
38. Kamel, A.A.: Perturbation Method in the Theory of Nonlinear Oscillations. *Celestial Mechanics* **3**, 90–106 (1970). DOI 10.1007/BF01230435
39. Kaula, W.M.: Development of the lunar and solar disturbing functions for a close satellite. *The Astronomical Journal* **67**, 300–303 (1962). DOI 10.1086/108729
40. Kelly, T.S.: A note on first-order normalizations of perturbed Keplerian systems. *Celestial Mechanics and Dynamical Astronomy* **46**, 19–25 (1989). DOI 10.1007/BF02426708
41. Kopp, G., Lean, J.L.: A new, lower value of total solar irradiance: Evidence and climate significance. *Geophysical Research Letters* **38**(1), L01706 (2011). DOI 10.1029/2010GL045777
42. Kozai, Y.: Effects of Solar Radiation Pressure on the Motion of an Artificial Satellite. *SAO Special Report* **56**, 25–34 (1961)
43. Kozai, Y.: Mean values of cosine functions in elliptic motion. *The Astronomical Journal* **67**, 311–312 (1962). DOI 10.1086/108731
44. Kozai, Y.: Second-order solution of artificial satellite theory without air drag. *The Astronomical Journal* **67**, 446–461 (1962). DOI 10.1086/108753
45. Krivov, A.V., Getino, J.: Orbital evolution of high-altitude balloon satellites. *Astronomy and Astrophysics* **318**, 308–314 (1997)
46. Kubo-oka, T., Sengoku, A.: Solar radiation pressure model for the relay satellite of SELENE. *Earth, Planets and Space* **51**, 979–986 (1999). DOI 10.1186/BF03351568
47. Kummer, M.: On resonant non linearly coupled oscillators with two equal frequencies. *Communications in Mathematical Physics* **48**, 53–79 (1976). DOI 10.1007/BF01609411. Erratum: *Communications in Mathematical Physics* **60**, 192 (1978).
48. Lara, M.: A Hopf variables view on the libration points dynamics. *Celestial Mechanics and Dynamical Astronomy* **129**(3), 285–306 (2017). DOI 10.1007/s10569-017-9778-4
49. Lara, M.: Solution to the main problem of the artificial satellite by reverse normalization. *Nonlinear Dynamics* **101**(2), 1501–1524 (2020). DOI 10.1007/s11071-020-05857-3
50. Lara, M.: Brouwer's satellite solution redux. *Celestial Mechanics and Dynamical Astronomy* **133**(47), 1–20 (2021). DOI 10.1007/s10569-021-10043-7

51. Lara, M.: Hamiltonian Perturbation Solutions for Spacecraft Orbit Prediction. The method of Lie Transforms, *De Gruyter Studies in Mathematical Physics*, vol. 54, 1 edn. De Gruyter, Berlin/Boston (2021). DOI 10.1515/9783110668513-006
52. Lara, M., Fantino, E., Flores, R.: Nonlinear Effects of the Central Body Oblateness on the Coplanar Dynamics of Solar Sails. In: W. Lacarbonara (ed.) *Advances in Nonlinear Dynamics*, Volume I, no. 12 in NODYCON Conference Proceedings. Springer Nature, Switzerland (2024). DOI 10.1007/978-3-031-50631-4_12. URL https://doi.org/10.1007/978-3-031-50631-4_12
53. Lara, M., Masat, A., Colombo, C.: A torsion-based solution to the hyperbolic regime of the J_2 -problem. *Nonlinear Dynamics* **111**, 9377–9393 (2023). DOI 10.1007/s11071-023-08325-w
54. Lara, M., Pérez, I.L., López, R.: Higher order approximation to the Hill problem dynamics about the libration points. *Communications in Nonlinear Science and Numerical Simulations* **59**, 612–628 (2018). DOI 10.1016/j.cnsns.2017.12.007
55. Lara, M., Rosengren, A.J., Fantino, E.: Non-singular recursion formulas for third-body perturbations in mean vectorial elements. *Astronomy and Astrophysics* **634**(Article A61), 1–9 (2020). DOI 10.1051/0004-6361/201937106
56. Lumme, K.: On the Formation of Saturn’s Rings. *Astrophysics and Space Science* **15**(3), 404–414 (1972). DOI 10.1007/BF00649769
57. Lyddane, R.H., Cohen, C.J.: Numerical comparison between Brouwer’s theory and solution by Cowell’s method for the orbit of an artificial satellite. *Astronomical Journal* **67**, 176–177 (1962). DOI 10.1086/108689
58. Marchesiello, A., Pucacco, G.: Bifurcation Sequences in the Symmetric 1:1 Hamiltonian Resonance. *International Journal of Bifurcation and Chaos* **26**, 1630011-1562 (2016). DOI 10.1142/S0218127416300111
59. Massé, C., Sharf, I., Deleflie, F.: Exploitation of STRP and J_2 perturbations for deorbitation of spacecraft through attitude control. *Acta Astronautica* **203**, 551–567 (2023). DOI 10.1016/j.actaastro.2022.12.008
60. McInnes, C.R.: *Solar sailing. Technology, dynamics and mission applications.*, 1st edn. Astronomy and Planetary Sciences. Springer, London (UK) (1999)
61. Meer van der, J.C., Cushman, R.: Orbiting dust under radiation pressure. In: H. Doebner, J. Hennig (eds.) *Proceedings of the XVth International Conference on Differential Geometric Methods in Theoretical Physics (Clausthal-Zellerfeld, Germany, 1986)*, pp. 403–414. World Scientific, Singapore (1987)
62. Mignard, F.: Radiation pressure and dust particle dynamics. *Icarus* **49**(3), 347–366 (1982). DOI 10.1016/0019-1035(82)90041-0
63. Mignard, F., Henon, M.: About an Unsuspected Integrable Problem. *Celestial Mechanics* **33**(3), 239–250 (1984). DOI 10.1007/BF01230506
64. Milani, A., Nobili, A.M., Farinella, P.: *Non-gravitational perturbations and satellite geodesy.* Adam Hilger Ltd., Bristol, UK (1987)
65. Montenbruck, O., Gill, E.: *Satellite Orbits. Models, Methods and Applications.* Physics and Astronomy. Springer-Verlag, Berlin, Heidelberg, New York (2001)
66. Musen, P.: The Influence of the Solar Radiation Pressure on the Motion of an Artificial Satellite. *Journal of Geophysical Research* **65**, 1391–1396 (1960). DOI 10.1029/JZ065i005p01391
67. Musen, P., Bryant, R., Bailie, A.: Perturbations in Perigee Height of Vanguard I. *Science* **131**, 935–936 (1960). DOI 10.1126/science.131.3404.935
68. Nayfeh, A.H.: *Perturbation Methods.* Wiley-VCH Verlag GmbH & Co. KGaA, Weinheim, Germany (2004)
69. Palacián, J.F., Vanegas, J., Yanguas, P.: Compact normalisations in the elliptic restricted three body problem. *Astrophysics and Space Science* **362**, 215 (2017). DOI 10.1007/s10509-017-3195-8
70. Parkinson, R.W., Jones, H.M., Shapiro, I.I.: Effects of solar radiation pressure on earth satellite orbits. *Science* **131**(3404), 920–921 (1960). DOI 10.1126/science.131.3404.920
71. Peale, S.J.: Dust belt of the Earth. *Journal of Geophysical Research* **71**(3), 911–933 (1966). DOI 10.1029/JZ071i003p00911
72. Plummer, H.C.: On the Possible Effects of Radiation on the Motion of Comets, with special reference to Encke’s Comet. *Monthly Notices of the Royal Astronomical Society* **65**, 229–238 (1905). DOI 10.1093/mnras/65.3.229
73. Poincaré, H.: *Les méthodes nouvelles de la mécanique céleste. Tome 2.* Gauthier-Villars et fils (Paris) (1893). URL <http://hdl.handle.net/1908/3852>
74. Pokorný, P., Deutsch, A.N., Kuchner, M.J.: Mercury’s Circumsolar Dust Ring as an Imprint of a Recent Impact. *The Planetary Science Journal* **4**(2), 33 (2023). DOI 10.3847/PSJ/acb52e
75. Robertson, H.P.: Dynamical Effects of Radiation in the Solar System. *Monthly Notices of the Royal Astronomical Society* **97**, 423–437 (1937). DOI 10.1093/mnras/97.6.423
76. San-Juan, J.F., López, R., Lara, M.: Vectorial formulation for the propagation of average dynamics under gravitational effects. *Acta Astronautica* **217**, 181–187 (2024). DOI 10.1016/j.actaastro.2024.01.018
77. Shapiro, I.I., Jones, H.M.: Perturbations of the Orbit of the Echo Balloon. *Science* **132**, 1484–1486 (1960). DOI 10.1126/science.132.3438.1484
78. Walter, H.G.: Conversion of osculating orbital elements into mean elements. *Astronomical Journal* **72**, 994–997 (1967). DOI 10.1086/110374
79. Zadunaisky, P.E., Shapiro, I.I., Jones, H.M.: Experimental and Theoretical Results on the Orbit of Echo 1. *SAO Special Report* **61** (1961)